J. Non-Newtonian Fluid Mech. xxx (2009) xxx–xxx

Contents lists available at ScienceDirect

Journal of Non-Newtonian Fluid Mechanics

journal homepage: www.elsevier.com/locate/jnnfm

Turbulent flow of viscoelastic shear-thinning liquids through a rectangular duct: Quantification of turbulence anisotropy

M.P. Escudier*, A.K. Nickson, R.J. Poole

Department of Engineering, University of Liverpool, Liverpool L69 3GH, UK

ARTICLE INFO

Article history:
Received 3 July 2008
Received in revised form 12 December 2008
Accepted 13 January 2009
Available online xxx

Keywords:
Drag-reduction
Shear-thinning polymer solutions
Rectangular duct
LDA

ABSTRACT

We report laser Doppler anemometry (LDA) measurements of mean velocity and turbulence structure for fully-developed turbulent flow through a rectangular duct of aqueous solutions of a xanthan gum and a polyacrylamide both of which are drag-reducing polymer solutions. All three components of the turbulent fluctuations (i.e. the Reynolds normal stresses) have been measured as well as the Reynolds shear stress $-\rho\overline{uv}$. A novel open-slit test-section allows measurement of the component of Reynolds normal stress perpendicular to the duct wall and of the Reynolds shear stress down to values of y^+, the distance from the surface in wall units, close to unity. We show that the maximum value of the transverse (or normal) component of turbulence intensity in wall units v'^+_{MAX} decreases linearly from about unity for zero drag reduction (DR_1) to about 0.6 at $DR_1 = 80\%$ while the lateral component w^+_{MAX} is practically independent of DR_1. For levels of drag reduction below 50% the streamwise component u'^+_{MAX} increases monotonically but for higher levels of drag reduction the trend is less clear. Anisotropy of the turbulence structure is characterised using Pope's modification [S. Pope, Turbulent flows (2000), Cambridge University Press, New York.] of the triangle plot suggested by Lumley [J.L. Lumley, Computational modelling of turbulent flows, Adv. Appl. Mech. 18 (1978) 123–176] and shown to follow closely the line for axisymmetric turbulence. The detailed LDA measurements are supplemented by particle-image velocimetry observations which reveal how drag reduction changes the near-wall streaky structure.

1. Introduction

It has been known for 60 years [1] that large reductions in turbulent frictional drag occur when high molecular-weight polymers, surfactants, etc. are added to a Newtonian solvent even at very low concentrations (as little as a few ppm). Recent advances in numerical modelling, especially Direct Numerical Simulations (e.g. [2–6]) have enhanced our understanding of how the additives interact with and modify the turbulence and reduce the frictional drag. At the same time, efforts are being made to develop modelling approaches to such flows which are far less demanding of computational resources and so suitable for routine engineering calculations in complex geometries (e.g. [7–9]). The purpose of the work presented here is to provide a more comprehensive experimental database than has been available hitherto to assist in the development and validation of both approaches, particularly for higher polymer concentrations where there are measurable differences in shear viscosity and other fluid properties when compared with the solvent and for which currently there are no data. Special emphasis here will be placed on the quantification of turbulence anisotropy which many previous studies have shown qualitatively is significantly different for drag-reducing liquid flows compared to the turbulent flow of a Newtonian fluid.

Previous experimental work, outlined in Table 1, on the turbulent flow of non-Newtonian liquids through a rectangular duct [10–24] is limited in several ways. Several of these studies [10–15] have been concerned with flow through square ducts where the low aspect ratio leads to a three-dimensional rather than a two-dimensional flow field and there may also be secondary-flow effects [14], particularly at low polymer concentrations for modestly drag-reducing additives where the turbulence structure (which drives the secondary motion for these inertia-dominated flows) may be only marginally different from that for a Newtonian fluid flow. There are, in addition, doubts about the validity of some of the very early data (e.g. [11] for which the u' values are roughly a factor of 2 higher than most comparable data). Ducts with aspect ratios in the range 10–19 are more typical [16–24] but in many cases the turbulence data are limited to the streamwise (or axial) component of velocity u'[1] [16], or the axial and normal v' components of velocity together with the Reynolds shear stress $-\rho\overline{uv}$ [17–23] but not the third com-

* Corresponding author.
E-mail address: m.p.escudier@liverpool.ac.uk (M.P. Escudier).

[1] In this paper u' represents the root-mean-square value of the fluctuating component of the streamwise (or axial) velocity component; v' is the rms value of the normal component of the fluctuating velocity and w' is the rms value of the lateral component.

0377-0257/$ – see front matter © 2009 Elsevier B.V. All rights reserved.
doi:10.1016/j.jnnfm.2009.01.002

Table 1
Summary of previous data (symbols correspond to data shown in Fig. 8).

Ref	Author(s)	Year	AR	Fluid(s)	Data	(Sets)
[10]	Logan	1972	1	50 ppm polyox	u', v', $\overline{uv}$	(2)
[11]	Rudd	1972	1	100 ppm PAA Separan AP30	u', v'	(1)
[16]	Reischman and Tiederman (☆)	1975	10.7	100 ppm PAA Separan AP273, 100 ppm Magnifloc 837A, 100 ppm Polyox WSR-301	u'	(3)
[24]	Gampert and Delgado (□)	1985	19	50 and 100 ppm PAA Praestol PR2850	u', v', w', $\overline{uv}$	(2)
[18]	Willmarth, Wei and Lee (Δ)	1987	12	10 ppm Polyox	u', v', $\overline{uv}$	(2)
[12]	Gampert and Yong	1988	1	50 and 100 ppm PAA Praestol 2360	u', v', $\overline{uv}$	(4)
[17]	Luchik and Tiederman (⊗)	1988	10	1.3 and 2.1 ppm PAA Separan AP273	u', v', $\overline{uv}$	(2)
[13]	Gampert and Yong (×)	1990	1	50 and 100 ppm PAA Praestol 2360	u', $\overline{uv}$	(4)
[19]	Harder and Tiederman (▽)	1991	10	3–5 ppm PAA Separan AP273	u', v', $\overline{uv}$	(2)
[20]	Wei and Wilmarth (▷)		11.9	10 ppm Polyox WSR-301	u', v', $\overline{uv}$	(3)
[21]	Gampert and Rensch (◁)	1996	1& 19	19 5–150 ppm PAA Praestol 2360	u', v', $\overline{uv}$	(23)
[22]	Warholic, Massah and Hanratty (+)	1999	12	0.25–50 ppm PAA Percol 727	u', v', $\overline{uv}$	(8)
[14]	Escudier and Smith (◊)	2001	1	0.1% CMC/0.1% XG, 0.125% PAA Separan AP273	u', v', w', $\overline{uv}$	(2)
[23]	Warholic, Heist, Katcher and Hanratty (○)	2001	12	1.24 and 50 ppm PAA Percol 727	u', v', $\overline{uv}$	(2)
[15]	Gampert, Braemar, Eich and Dietmann (♣)	2004	1	100 ppm–0.015% PAA Praestol 2300, 50–400 ppm XG	u', v', $\overline{uv}$	(8)

ponent of velocity w'. In fact, we have identified only one previous study [24] which also includes measurements of w': as will be discussed later, all three components of velocity are required, together with the Reynolds shear stress, if the turbulence anisotropy is to be quantified. With one exception [23], in which particle-image velocimetry was used, all previous measurements were made using laser Doppler anemometry. A further limitation of previous work is to relatively low polymer concentrations where the liquid viscosity is essentially that of the solvent (invariably water). Even where the concentration has been sufficiently high to significantly change the liquid rheology, little information is given about the viscosity-shear rate curve. In only two cases, [15] and [22], are flow curves provided to quantify the degree of shear thinning though in the former paper the viscosity data for high shear rates were affected by Taylor instabilities and in both cases the ratio of maximum to minimum shear viscosity was less than 20. Finally, in many instances the data provided are very limited (e.g. a single set of profiles), incomplete (e.g. no information about wall shear stress or bulk velocity) or of questionable accuracy (e.g. measured values of friction factor for a Newtonian fluid significantly different from values calculated from well-established correlations [26]).

2. Experimental arrangement and instrumentation

Although new, the flowloop used here is similar in design to facilities used in previous research at the University of Liverpool [7,14,25]. The new loop incorporates a rectangular duct comprising six 1.2m long stainless-steel modules with an internal cross-section of height $H = 25$ mm and width $w = 298$ mm (hydraulic diameter $D_H = 2wH/(w + H) = 46$ mm, aspect ratio $w/h = 11.92$). Five of the modules are upstream of the Perspex, stainless-steel and glass test section, length 250 mm, which is therefore located 6 m ($240H$) from the duct inlet. Flow is provided by a progressive cavity pump, Mono type E101, with a maximum flowrate of 0.025 m^3/s. The flow rate was measured by an Endress and Hauser Promag P electromagnetic flowmeter. The flow enters and leaves the rectangular duct through transition sections which change gradually in cross-section from circular to rectangular and vice versa.

In the test section, shown schematically in Fig. 1, a unique open-slot arrangement, inspired by the open-channel work of Poggi et al (2002) [27], allows essentially unimpeded access of the LDA laser beams to the flowing liquid. This technique permits simultaneous and coincident measurement of the mean axial velocity u, the RMS value of the fluctuating axial velocity component u' and the RMS fluctuating velocity component normal to the duct surface v', and hence the determination of the Reynolds shear stress $-\rho\overline{uv}$, without the need for a complex optical arrangement such as has been used in the past (e.g. [18–20],). The third fluctuating velocity component w', orthogonal to u' and v', was measured separately. The streamwise velocity was remeasured simultaneously with the w' data to provide both a consistency check and a way of monitoring polymer degradation. A Dantec FibreFlow 2D LDA system, comprising a 60×10 probe and 55X12 beam expander together with Dantec BSA 57N20 and 57N10 burst spectrum analyser signal processors was used to measure the distributions of the mean and fluctuating velocities. The optical system produces a measuring volume with length 180 μm and diameter 20 μm. The streamwise pressure gradient was estimated from measurements of the pressure difference between pressure tappings installed in the stainless-steel modules (i.e. with 1.2 m separation) using a Validyne DP15-30 pressure transducer linked to a Validyne CD223 digital indicator. The pressure transducer was calibrated periodically against an MKS Baratron differential pressure transducer (1000 torr fsd). Fluid temperature was monitored using a platinum-resistance thermometer installed at the downstream end of the duct.

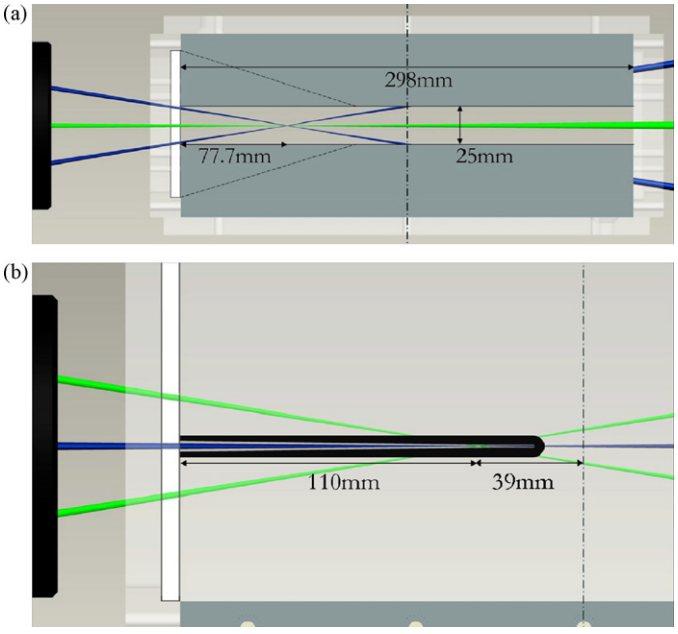

Fig. 1. Schematic of the test section showing the LDA access slit: (a) cross-section, (b) plan view.

Please cite this article in press as: M.P. Escudier, et al., Turbulent flow of viscoelastic shear-thinning liquids through a rectangular duct: Quantification of turbulence anisotropy, J. Non-Newtonian Fluid Mech. (2009), doi:10.1016/j.jnnfm.2009.01.002

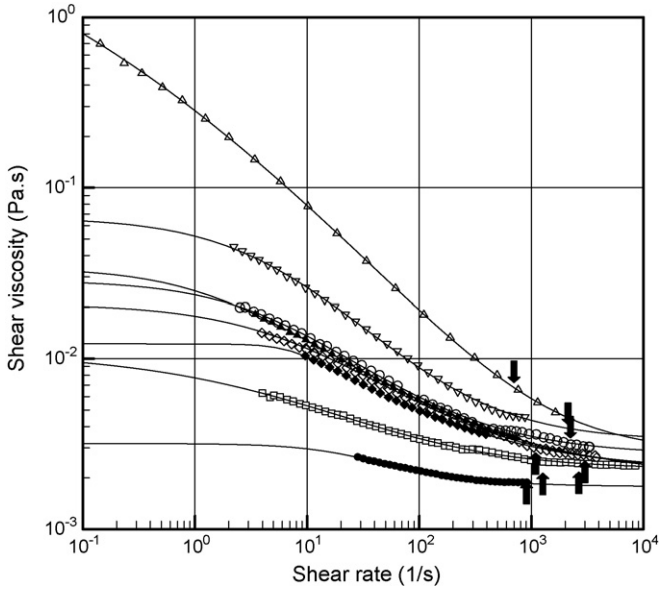

Fig. 2. Flow curves for xanthan gum (XG) and polyacrylamide (PAA) with Carreau–Yasuda fits (parameter values listed in Table 2). Arrows indicate approximate wall shear rates for the detailed LDA measurements.

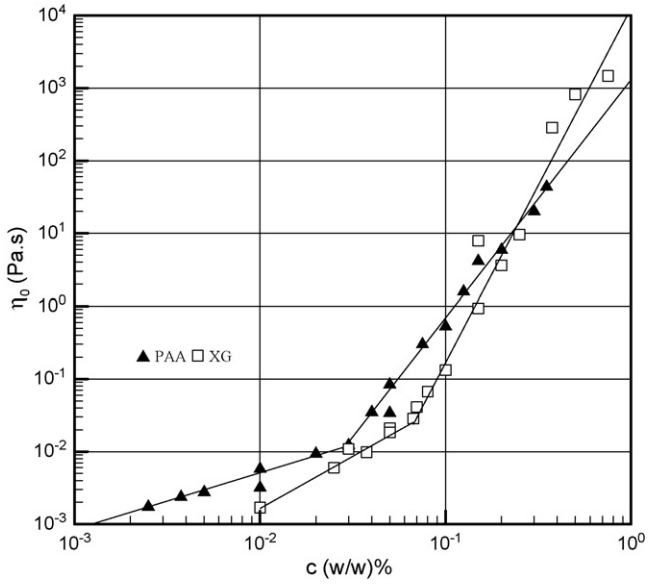

Fig. 3. Determination of critical overlap concentrations c^* ▲ PAA □ XG.

PIV observations in planes parallel to the upper surface of the duct were made using a Dantec two-component DC-PIV system with a New Wave Research 50 mJ double-pulsed Nd:YAG laser. The PIV observations were carried out using 50 μm polyamid seeding particles. The distance of the laser sheet from the surface was set by passing it through a long 1 mm wide slit cut into a mask which was positioned in front of the test section and adjustable vertically.

3. Fluid rheology and critical overlap concentration

The non-Newtonian test liquids were aqueous solutions of two polymers. The first was a polyacrylamide, Separan AP 273 E Supplied by Floerger—hereafter PAA, which is regarded as having a highly flexible molecular structure [28] and so is strongly viscoelastic and drag reducing. The second fluid was a xanthan gum (Keltrol TF supplied by Kelco Ltd.—hereafter XG) which, having a more rigid-rod-like structure, is less viscoelastic in the non-linear regime and also less drag reducing [25]. Measurements of the flow curves (shear viscosity vs shear rate) for these liquids were carried out with a TA Instruments AR1000N controlled-stress rheometer using a cone and plate geometry (60 mm diameter, 2° cone angle) for low-medium shear rates, a 40 mm diameter parallel-plate geometry at high shear rates and a double-concentric cylinder arrangement at very low shear rates (diameters 20.00, 20.38, 21.96 and 22.38 mm). The shear-thinning character of the fluids is evident from Fig. 2 as is the fact that the data are well fitted by the Carreau–Yasuda model:

$$\frac{\mu-\mu_\infty}{\mu_0-\mu_\infty}=\frac{1}{[1+(\lambda\dot{\gamma})^a]^{n/a}}. \quad (1)$$

In Eq. (1) μ_0 is the zero-shear-rate viscosity, μ_∞ is the infinite-shear-rate viscosity, λ is a constant (with dimensions of time) which characterises the onset of shear thinning, n is a power-law index and a is a fitting parameter introduced by Yasuda et al. [29]. The resulting values of μ_0 plotted versus concentration c in Fig. 3 in log-log form, show well-defined power-law variations, $\mu_0 \propto c^m$, with different values of the exponent m for each polymer, above and below the critical overlap concentration c^*. Fluids with $c<c^*$ are designated dilute (i.e. the molecules are sufficiently far apart that there are minimal interactions between them) and those with $c>c^*$ as semi dilute. For XG, we find $c^*\approx 0.067\%$ and for PAA $c^*\approx 0.03\%$. The turbulence data presented here are for the flow of both dilute and semi dilute solutions: XG in the range 0.03–0.15% with levels of drag reduction (see below) in the range 33–67%, PAA in the range 0.01–0.05% and drag reduction 65–75%. Values for all the Carreau–Yasuda parameters for the working fluids used here are listed in Table 2.

We used a Capillary Break-up Extensional Rheometer (CaBER) to obtain characteristic times for uniaxial extensional stress growth for the two higher concentrations of the polyacrylamide solutions: 25 ms (0.03%) and 56 ms (0.05%). Unfortunately for the xanthan gum solutions the concentrations were too low to enable any meaningful data to be extracted. Given the incompleteness of the extensional-flow data, it would be impossible to speculate how strain-hardening might influence the turbulence structure. Nevertheless we include these two values in the hope that this limited relaxation-time data for PAA may be useful for modellers wishing to simulate our results.

4. Friction factor versus Reynolds number

The Fanning friction factor $f\equiv 2\tau_W/\rho U^2$ is shown in Fig. 4(a) (xanthan gum, XG) and 4(b) (polyacrylamide, PAA) plotted against a Reynolds number defined as $Re\equiv \rho HU/2\,\mu_W$ where ρ is the fluid density (taken to be the same as that of the solvent, water), H is

Table 2
Carreau–Yasuda parameters for all liquids.

Symbols used in Figs. 5, 6, 9, 10, 11 and 12	XG △	XG ▽	XG ○	XG ◊	XG □	PAA ▲	PAA ♦	PAA ●
μ_0 (Pa s)	7.87	3.27	0.0287	0.0209	0.0109	0.034	0.0122	0.00318
μ_∞ (Pa s)	0.00284	0.00293	0.00274	0.00226	0.00227	0.00202	0.00215	0.00178
λ (s)	4.29	12.2	0.232	0.141	0.095	0.740	0.137	0.040
n	0.880	0.795	0.664	0.614	0.689	0.498	0.487	0.802
a	0.231	0.213	0.801	0.719	0.447	0.852	2.73	1.29

Please cite this article in press as: M.P. Escudier, et al., Turbulent flow of viscoelastic shear-thinning liquids through a rectangular duct: Quantification of turbulence anisotropy, J. Non-Newtonian Fluid Mech. (2009), doi:10.1016/j.jnnfm.2009.01.002

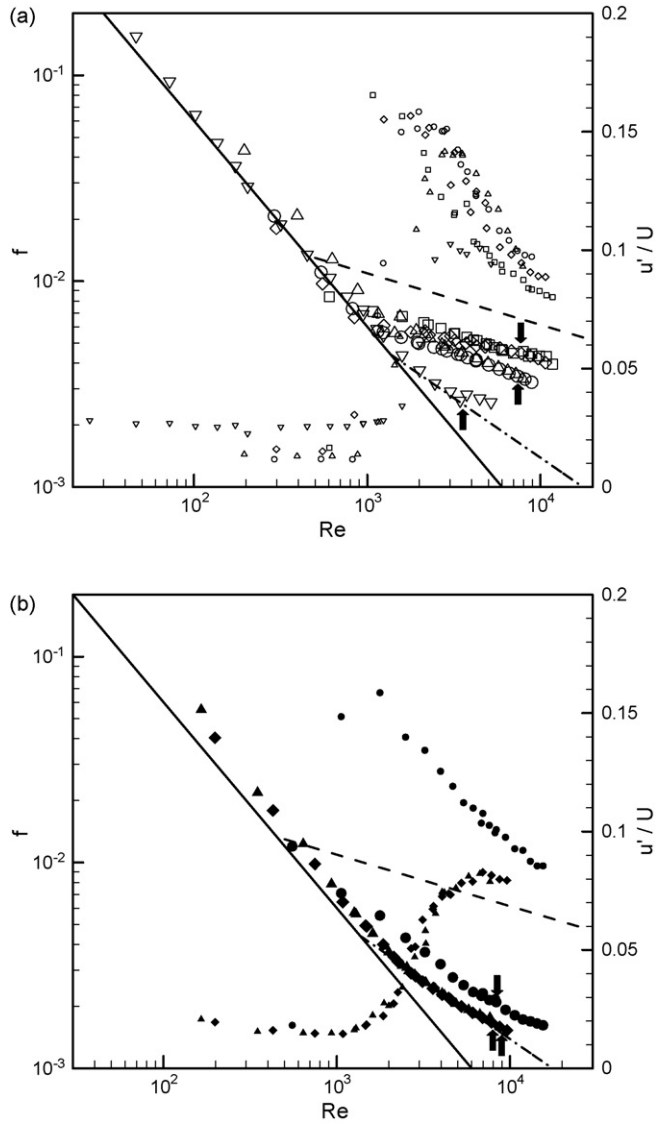

Fig. 4. (a) *f-Re* plots for XG data sets including near-wall fluctuation level to indicate transition. Large symbols: *f-Re* data. Small symbols: u'/U data. Arrows indicate approximate Reynolds numbers of the detailed LDA measurements. (b) *f-Re* plots for PAA data sets including near-wall fluctuation level to indicate transition. Large symbols: *f-Re* data. Small symbols: u'/U data. Arrows indicate approximate Reynolds numbers of the detailed LDA measurements.

the channel height, U is the bulk mean velocity, and μ_W is the near-wall viscosity determined from the wall shear stress τ_W and the Carreau–Yasuda model fits. The wall shear stress was determined from pressure-drop measurements. Also shown on each figure is

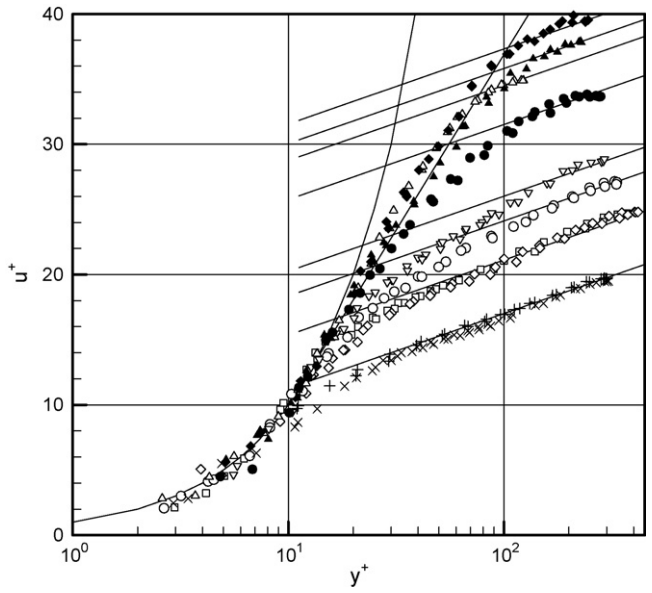

Fig. 5. Mean velocity profiles in wall coordinates u^+ vs log y^+ for all data: + water, × glycerol, □ 0.03% XG, ◊ 0.05% XG, ○ 0.067% XG, ▽ 0.08% XG, △ 0.15% XG, ● 0.01% PAA, ♦ 0.03% PAA, ▲ 0.05% PAA. Associated flow parameter values are listed in Table 3.

the near-wall ($y = 2.5$ mm, $y/H = 0.1$) streamwise component of turbulence intensity u' which we have shown in previous work [25] is an excellent indicator of laminar-turbulent transition whereas in general the $f(Re)$ curves are not. The solid straight line for the laminar flow regime corresponds to $f.Re = 21.6$, appropriate for the fully-developed flow of a Newtonian fluid through a rectangular duct with an aspect ratio of 12. The dashed line represents the correlation of Dean [26]

$$\text{i.e.} \qquad f_N = 0.073(\rho UH/\mu)^{-0.25} \tag{2}$$

The lower curve represents Virk's (1975) drag-reduction asymptote for pipe flow [30] transformed to a form applicable to a rectangular duct using a procedure based upon that suggested by Kozicki and Tiu [31]

$$\text{i.e.} \qquad \frac{1}{\sqrt{f_V}} = 19\log_{10}\left(Re^*\sqrt{f_V}\right) - 32.4 \tag{3}$$

where the subscript V refers to Virk, $Re^* = Re/d$ and, for an aspect ratio of 12, the geometric factor d takes the value 1.3474 [31].

An interesting feature of the XG data is that the *f-Re* data for 0.03% and 0.05% collapse, the data for 0.067% and 0.08% are slightly lower but also collapse, and the data for 0.15% are considerably lower and close to Virk's asymptote. For PAA the data for 0.03% and 0.05% are practically identical and, in the turbulent-flow regime, follow Virk's asymptote while the *f-Re* data for 0.01% show much

Table 3
Fluid and flow parameters.

Symbols used in Figs. 5, 6, 9, 10, 11 and 12	Water +	Glycerol ×	XG △	XG ▽	XG ○	XG ◊	XG □	PAA ▲	PAA ♦	PAA ●
Concentration (%)	–	45	0.15	0.08	0.067	0.05	0.03	0.05	0.03	0.01
c/c^*	–	–	2.24	1.19	1.00	0.75	0.45	1.67	1.00	0.33
U (m/s)	0.41	1.82	1.93	2.24	2.00	1.91	1.67	1.92	2.09	1.22
τ_W (Pa)	0.61	13.1	4.90	8.20	7.17	7.89	6.01	3.36	3.45	1.66
μ_W (Pa s)	0.001	0.0049	0.0070	0.0039	0.0032	0.0028	0.0024	0.0032	0.0030	0.0019
ρ (kg/m^3)	1000	1107	1000	1000	1000	1000	1000	1000	1000	1000
u_τ (m/s)	0.025	0.109	0.070	0.091	0.085	0.089	0.078	0.058	0.059	0.041
Re	5100	5100	3500	7300	7600	7300	7900	8000	8800	8300
f	0.0073	0.0073	0.0027	0.0036	0.0036	0.0043	0.0043	0.0018	0.0016	0.0022
DR_1 (%)	–	–	67	49	45	35	33	72	75	65
Re_τ	313	307	174	253	332	408	397	234	253	274
DR_2 (%)	–	–	67	59	52	40	42	74	77	74

Please cite this article in press as: M.P. Escudier, et al., Turbulent flow of viscoelastic shear-thinning liquids through a rectangular duct: Quantification of turbulence anisotropy, J. Non-Newtonian Fluid Mech. (2009), doi:10.1016/j.jnnfm.2009.01.002

less drag reduction and the turbulence intensity data reach very high levels at the end of transition.

Percentage drag reduction is defined as

$$DR = 100\left(1 - \frac{f}{f_N}\right) \tag{4}$$

where f and f_N are determined at either the same value of Re, yielding drag reduction DR_1, or the same value of $Re_\tau \equiv \rho H u_\tau / 2\mu_W$, where $u_\tau \equiv \sqrt{\tau_W/\rho}$ is the friction velocity, which yields DR_2. The particular value of Re at which the detailed LDA measurements were made is indicated on each $f(Re)$ curve. The values of both DR_1 and DR_2 corresponding to the detailed measurements are included in Table 3 together with all other basic flow and fluid properties as well as the symbols used in subsequent figures. We note that because all the non-Newtonian fluids under consideration here are shear thinning, some by as much as two orders of magnitude in shear viscosity, quantifying the degree of drag reduction is less straightforward than for situations where the polymer concentration is so low that the fluid viscosity is taken to be that of the solvent. In particular, instead of μ_W the reference viscosity used in the Reynolds number definitions could have been calculated for a characteristic shear rate $2U/H$ or the zero-shear-rate viscosity μ_0. To a certain degree, therefore, the degree of drag reduction is somewhat arbitrary although, as can be seen, the differences between the DR_1 and DR_2 values are generally quite small. This issue has been discussed previously [32] with conclusions consistent with those reached here.

5. Mean-velocity profiles

The quality of the detailed data is apparent from Fig. 5 which shows the mean-velocity distributions plotted in wall coordinates $u^+ \equiv u/u_\tau$ and $y^+ \equiv \rho u_\tau y/\mu_W$. For the Newtonian control fluids, water and 45% glycerol, the data closely follow the standard log law, $u^+ = 1/\kappa \ln y^+ + B$ with $\kappa = 0.4$ and $B = 5.5$, for $y^+ > 30$ and extend down to $y^+ \approx 3$. For PAA there are upshifts in the log-law region between $\Delta u^+ = 14$ and 21 depending upon the level of drag reduction while for XG $\Delta u^+ = 4$ to 18. The data for XG follow $u^+ = y^+$ from $y^+ \approx 1$ to

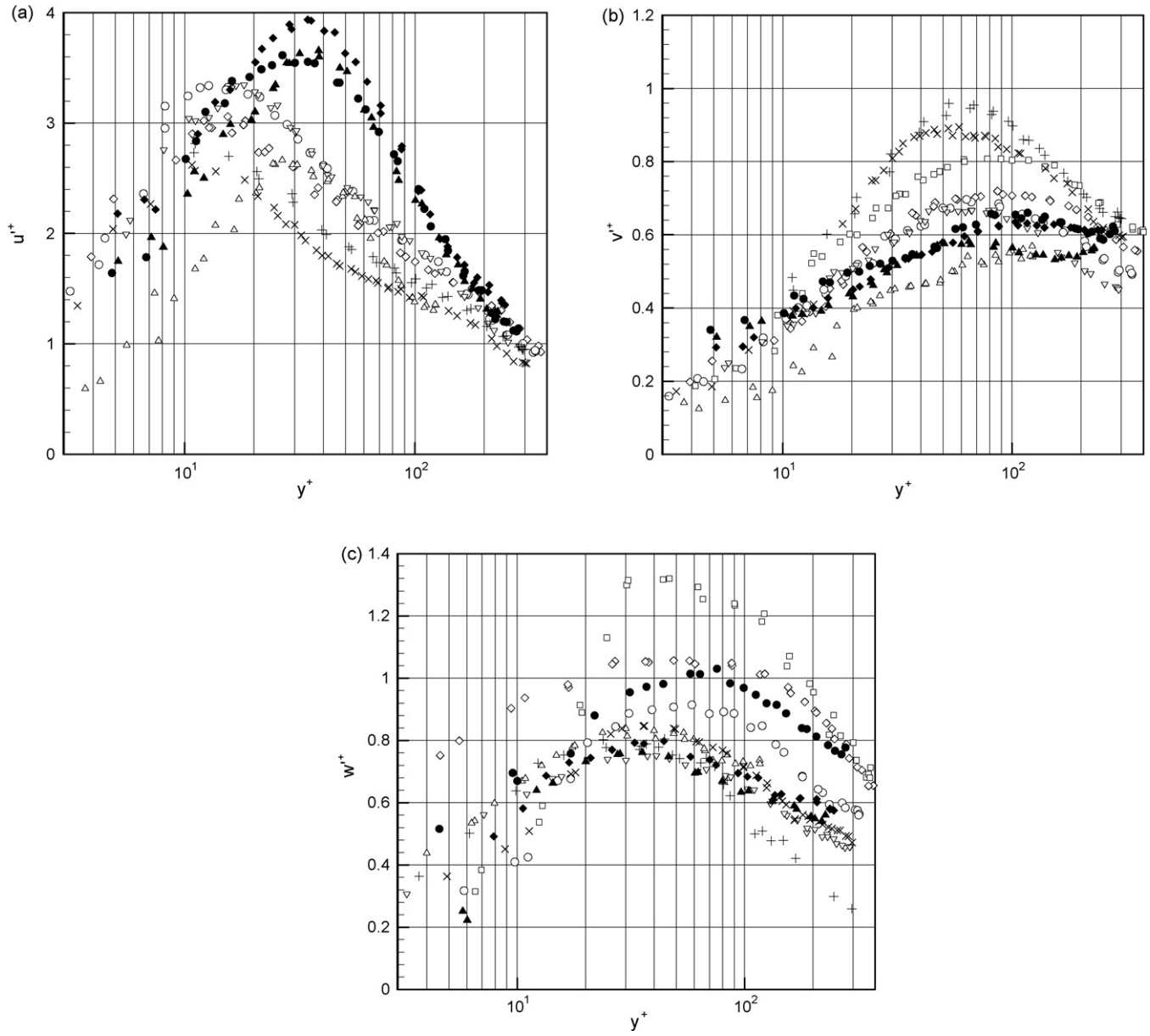

Fig. 6. (a) Reynolds' normal stress profiles in wall coordinates, u'^+. (b) Reynolds' normal stress profiles in wall coordinates, v'^+ (c) Reynolds' normal stress profiles in wall coordinates, w'^+.

Please cite this article in press as: M.P. Escudier, et al., Turbulent flow of viscoelastic shear-thinning liquids through a rectangular duct: Quantification of turbulence anisotropy, J. Non-Newtonian Fluid Mech. (2009), doi:10.1016/j.jnnfm.2009.01.002

ca 15 and for the highest concentration lie close to Virk's ultimate profile [30], $u^+ = 11.7 \ln y^+ - 17$. For PAA the data extend down to $y^+ \approx 5$ and again follow Virk's profile for the highest concentration. It is important to note that the sub-layer data confirm that the surface slit has no discernible influence on the flow. In each case, the smallest y-value is 0.5 mm corresponding to y^+ values in the range 1–5.

6. Normal Reynolds-stress and turbulent kinetic-energy profiles

The distributions of the rms values of the velocity fluctuations in the three orthogonal directions, $u'(y)$, $v'(y)$ and $w'(y)$ correspond to the three normal Reynolds-stresses. The distributions of these quantities are shown in Fig. 6 in wall coordinates: u'^+ vs y^+ in Fig. 6(a), v'^+ vs y^+ in Fig. 6(b) and w'^+ vs y^+ in Fig. 6(c). The trends are more easily discerned in Fig. 7 where the peak values of each of the normalised normal Reynolds stresses and the peak locations are plotted versus the level of drag reduction in Fig. 7(a) and (b), respectively. For the axial component of the fluctuating velocity u'^+ it is clear that in general the peak increases with drag reduction (DR_1) with the exception of the point for 0.15% XG at $DR_1 = 67\%$, possibly because these data are for a significantly lower Reynolds number (3500 compared with about 8000 for the other polymer solutions). The trend for v'^+ is also clear essentially decreasing linearly from about unity for zero drag reduction (DR_1) to about 0.6 at $DR_1 = 80\%$. The trends for w'^+ are more complex with the data for both XG and PAA exhibiting a decrease followed by an increase with increasing DR_1 but from levels above that for the Newtonian fluid flow, considerably so in the case of XG where the peak value for the lowest concentration ($c = 0.03\%$, $DR_1 = 33\%$) is 1.32. Both v'^+ and w'^+ are roughly equal to unity while u'^+ generally has values in the range 2.7 to 4.0. Since u_τ inevitably decreases with increasing DR_1, as the wall-shear stress decreases, it is apparent that w' itself decreases roughly in proportion to u_τ. Overall the data in Fig. 7(a) suggest an increased level of anistropy with increasing DR_1 and this will be confirmed when we address this specific issue later.

Fig. 8, which shows the data in Fig. 7(a) together with all other available data (i.e. those included in Table 1), confirms that the peak values of v'^+ and w' are both of order unity but while the limited data available suggest that w'^+_{MAX} is essentially unaffected by the level of drag reduction, v'^+_{MAX} decreases almost linearly with DR_1 by about 40% between zero and 80% drag reduction. The situation for u'^+ is more complicated: for levels of drag reduction below about 50%, u'^+_{MAX} increases monotonically with DR_1 although clearly there is a great deal of scatter in the data. To some extent this is probably a consequence of the inclusion of square-duct data as well as such sources of experimental uncertainty as gradient broadening etc. However the occurrence of a significant number of data points with low peak values at high drag reduction is almost certainly an indication that in addition to v'^+, drag reduction is ultimately accompanied by suppression of u'^+.

Fig. 7(b) shows that in terms of wall units, the u'^+ peak moves progressively away from the wall which corresponds to the well known tendency for an increase in the thickness of the viscous sublayer and buffer region also evident from the mean velocity data in Fig. 5. The data for the peak locations of both v'^+ and w'^+ are again complex with no obvious consistency. For XG the v'^+ peak moves

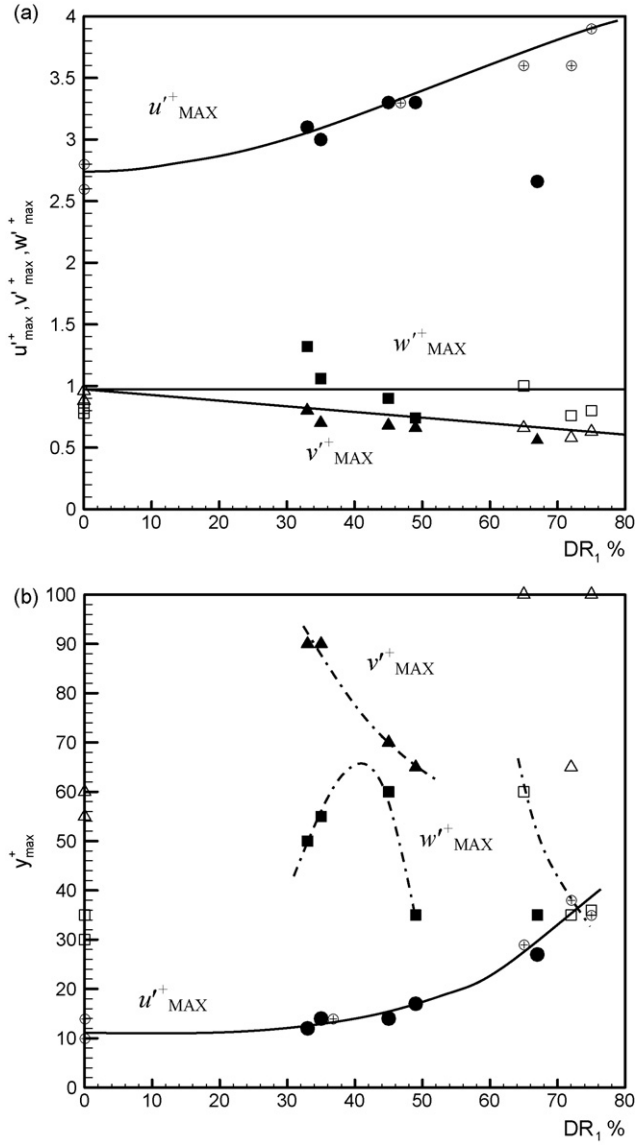

Fig. 7. (a) Peak values of u'^+, v'^+ and w'^+ vs level of drag reduction DR_1. Filled points represent XG data. Hollow symbols represent PAA data. (b) Locations of peak values of u'^+, v'^+ and w'^+ vs level of drag reduction DR_1. Filled points represent XG data. Hollow symbols represent PAA data. No max v'^+ data point for 0.15% XG (DR = 67%).

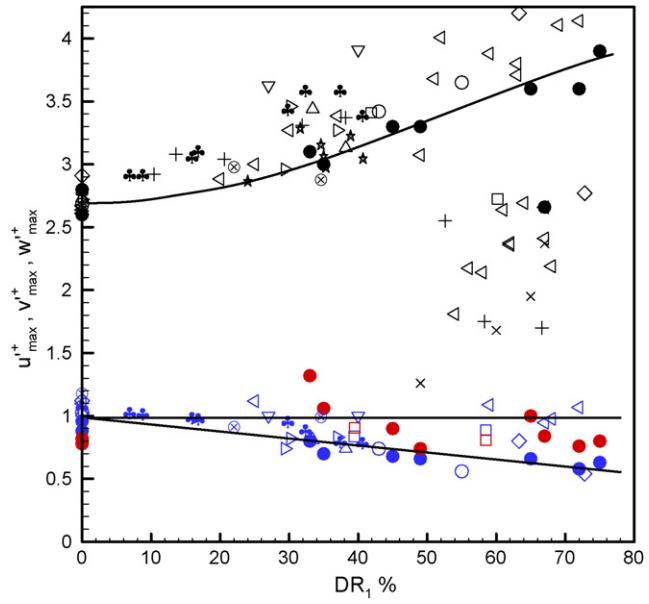

Fig. 8. Peak values of u'^+ (black symbols), v'^+ (blue symbols) and w'^+ (red symbols) vs level of drag reduction DR_1 for all studies listed in Table 1 (symbols identified in Table 1) including current data (filled circles). (For interpretation of the references to color in this figure legend, the reader is referred to the web version of the article.)

Please cite this article in press as: M.P. Escudier, et al., Turbulent flow of viscoelastic shear-thinning liquids through a rectangular duct: Quantification of turbulence anisotropy, J. Non-Newtonian Fluid Mech. (2009), doi:10.1016/j.jnnfm.2009.01.002

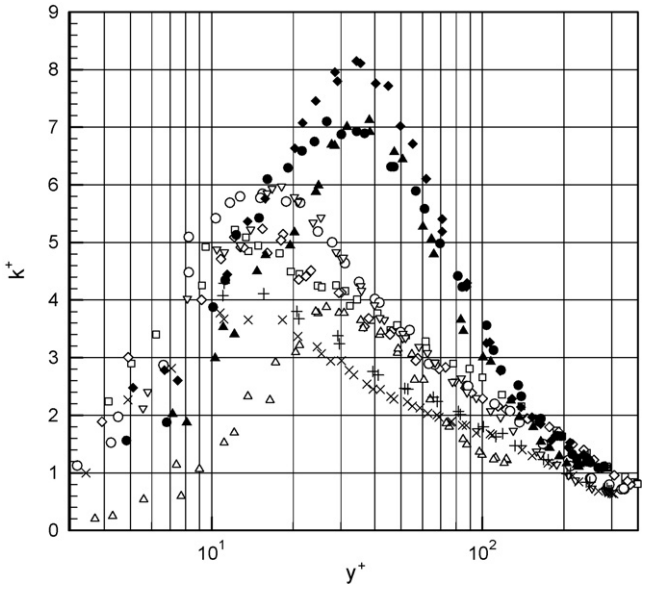

Fig. 9. Turbulent kinetic energy profiles in wall coordinates, k^+.

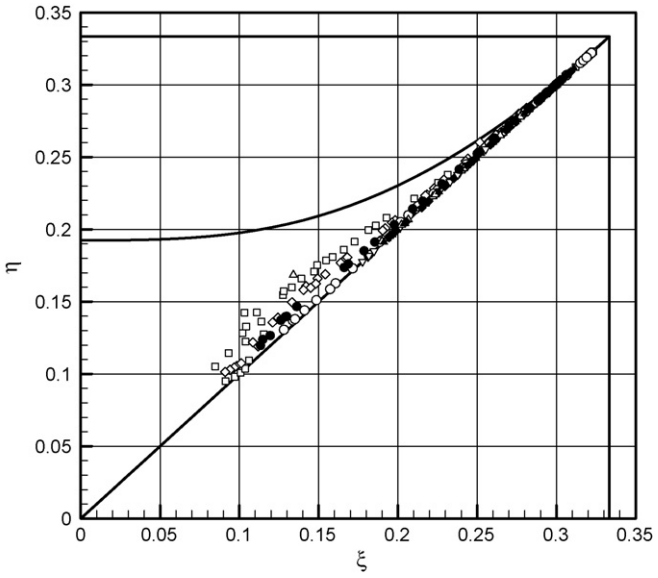

Fig. 11. Lumley–Pope triangle plot of anisotropy data η vs ξ.

closer to the wall as DR_1 increases but again starts from a higher level than the data for the Newtonian fluid flows. For PAA all three data points are above the level for the Newtonian fluid flow but show no clear trend. The w'^+ data for XG and PAA (excepting the low *Re* point for 0.15% XG) show quite opposite trends, with the peak for XG moving away from the wall and that for PAA towards the wall with increasing DR_1, both again starting from higher levels than for the Newtonian liquids. The data from previous studies are equally inconsistent and so not included here.

The distributions of turbulent kinetic energy k^+ (Fig. 9), are little different from those of u'^+, which is as expected as the principal contribution to k is generally u'^2.

7. Reynolds shear stress

For any fully-developed flow, the variation of total shear stress τ_T must follow the diagonal straight line included in Fig. 10. For a Newtonian fluid, the difference $\tau_T + \rho\overline{uv}$ equals the viscous contribution $\mu\partial u/\partial y$. For polymer solutions, the difference $\tau_T + \rho\overline{uv} - \mu\partial u/\partial y$ has to be compensated for by the so-called polymer stress. The reduction in v' discussed earlier together with the reduced correlation between u' and v' both lead to considerably reduced values of $-\rho\overline{uv}$ making accurate measurement of $-\rho\overline{uv}$ difficult. The increased uncertainty and scatter in the data of Fig. 10 are a consequence of this difficulty.

8. Turbulence anisotropy

All turbulent flows of practical interest are anisotropic to varying degrees and it has long been stated that the anisotropy is higher for drag-reducing liquids than it is for Newtonian fluids though this has rarely, if ever, been properly quantified. It is, however, a key characteristic which must be predicted in any numerical simulation of drag-reducing liquid flow. Since we have measured all three Reynolds normal stresses and the only non-zero Reynolds shear stress, we are in a position to compute η and ξ, the variables of the

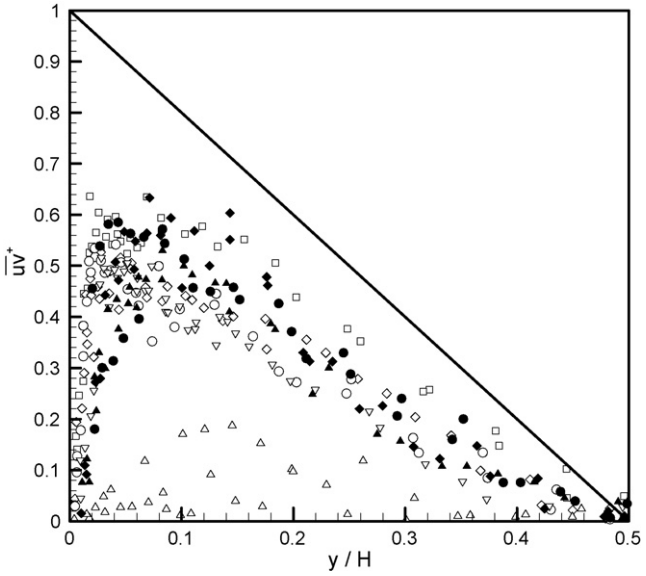

Fig. 10. Reynolds' shear stress profiles $(\overline{uv})^+$ vs *y/H*.

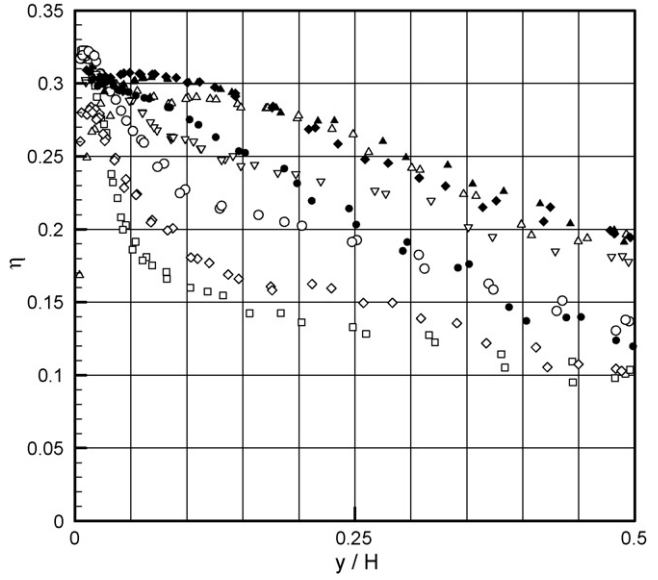

Fig. 12. Distributions of anistropy parameter η versus *y/H*.

Please cite this article in press as: M.P. Escudier, et al., Turbulent flow of viscoelastic shear-thinning liquids through a rectangular duct: Quantification of turbulence anisotropy, J. Non-Newtonian Fluid Mech. (2009), doi:10.1016/j.jnnfm.2009.01.002

Lumley "triangle" [33] in the modified form suggested recently by Pope [34]

$$\eta^2 = \frac{1}{6}\left[\frac{\left(\overline{u'^2}\right)^2 + \left(\overline{v'^2}\right)^2 + \left(\overline{w'^2}\right)^2}{4k^2} - \frac{1}{3} + \frac{(\overline{uv})^2}{2k^2}\right]$$

$$\xi^3 = \frac{1}{6}\left[\left(\frac{\overline{u'^2}}{2k} - \frac{1}{3}\right)^3 + \left(\frac{\overline{v'^2}}{2k} - \frac{1}{3}\right)^3 + \left(\frac{\overline{w'^2}}{2k} - \frac{1}{3}\right)^3 + \frac{3(\overline{uv})^2}{4k^2}\left[\frac{\overline{u'^2} + \overline{v'^2}}{2k} - \frac{2}{3}\right]\right]. \quad (5)$$

A more intuitive measure of anisotropy involving only the Reynolds normal stresses (i.e. with $\overline{uv}$ in the equation for η set equal to zero) is little different from η for the flows under discussion here. It should be emphasised that the Reynolds stresses at any point in a physically realizable turbulent flow will lead to values of η and ξ which correspond to a point within the Lumley–Pope triangle. All the XG and PAA data are shown in Fig. 11 and the extent to which they follow the side of the triangle representing axisymmetric turbulence ($\eta = \xi$) is quite remarkable. Closer examination reveals that the PAA data deviate slightly from the $\eta = \xi$ line for 0.01% PAA while for XG the trend as the concentration decreases is for increasing deviation towards the upper (curved) side of the triangle, which represents two-component turbulence. It has been argued recently [34] that this behaviour for drag-reducing fluid flows is a consequence of rolled-up polymer chains being partially unrolled and

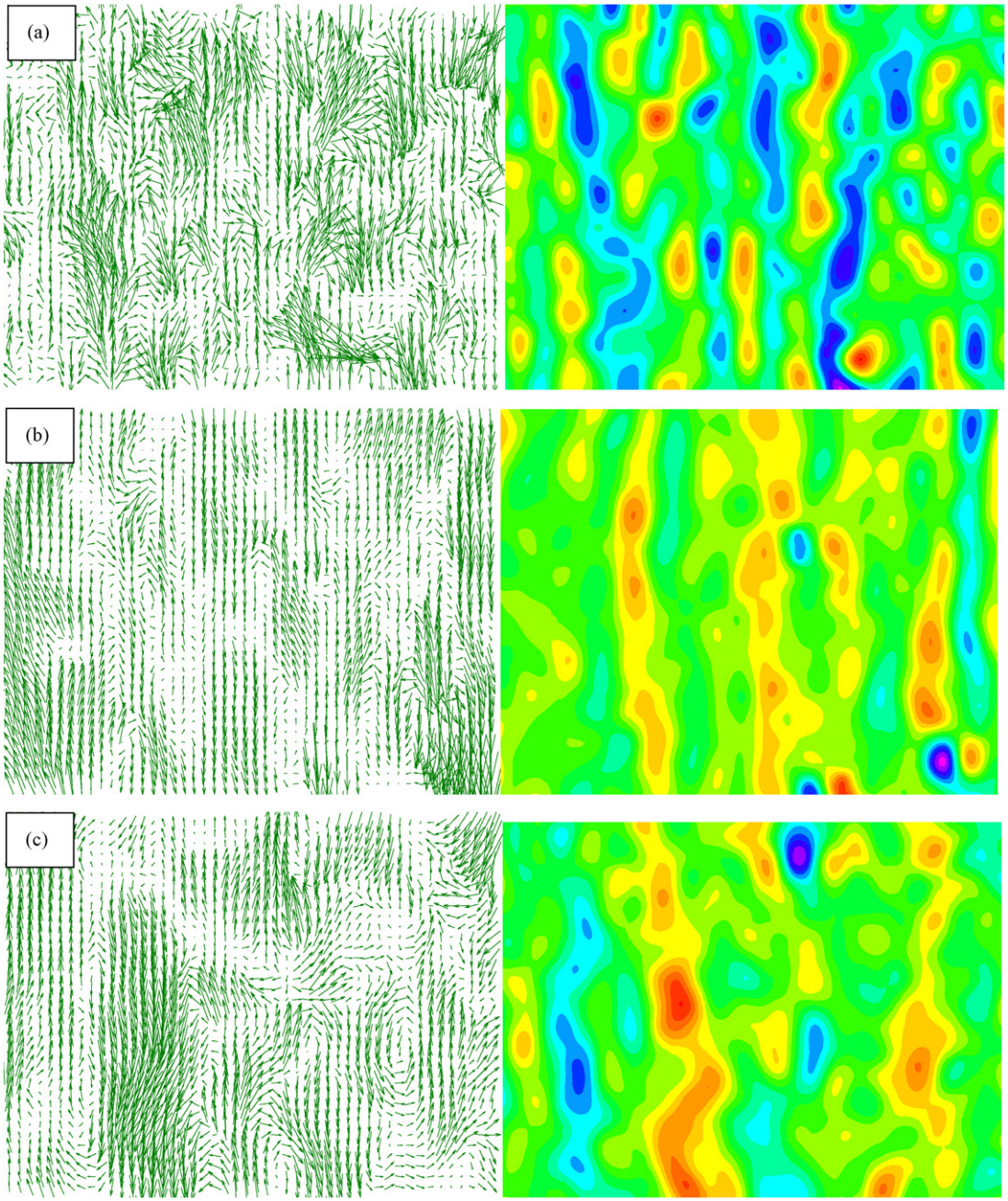

Fig. 13. PIV results: vector maps of instantaneous fluctuating velocity vectors (LHS) and instantaneous vorticity contours (RHS). Flow direction is bottom to top. (a) 45% GLY 0.5 mm from top surface ($y^+ = 12$), (b) 0.08% XG 1 mm from top surface ($y^+ = 23$) and (c) 0.03%PAA 5 mm from top surface ($y^+ = 101$). (For interpretation of the references to color in this figure legend, the reader is referred to the web version of the article.)

Please cite this article in press as: M.P. Escudier, et al., Turbulent flow of viscoelastic shear-thinning liquids through a rectangular duct: Quantification of turbulence anisotropy, J. Non-Newtonian Fluid Mech. (2009), doi:10.1016/j.jnnfm.2009.01.002

stretched in the mean-flow direction. The data presented here are consistent with the pipe-flow data of [35] for much more dilute (5 and 10 ppm PAA) polymer solutions.

The η-values plotted versus y/H in Fig. 12 show more clearly how the degree of isotropy increases (i.e. η falls) with distance from the duct surface. The maximum possible value for η (and also ξ) is 1/3, corresponding to one-dimensional turbulence. The peak values here are very close to the maximum, consistent with the rapid reduction of v' and w' with approach to a surface but in no case do the data follow the two-dimensional turbulence line (the curved top side of the Lumley–Pope triangle). In all cases, the highest level of anisotropy is closer to the surface than the peak in the turbulent kinetic energy which moves progressively away from the surface with increasing levels of drag reduction (as shown in Fig. 9). Since the four Reynolds stresses peak at different y-locations, it is not surprising that the peak in η is at a different location to the peak in k.

9. PIV observations

Sample PIV observations are shown for 45% glycerine (Fig. 13(a)), 0.08% XG (Fig. 13(b)) and 0.03% PAA (Fig. 13(c)). In each case the data were recorded at a y-location close to the peak u'^+ location for the particular flow concerned. The data have been processed to yield a vector map of the instantaneous fluctuating velocity vectors (i.e. the mean has been subtracted) in an x-z plane and the corresponding instantaneous vorticity contours in the same plane. The streamwise flow direction in each figure is "upwards". The streaky structure of the flow in each case is immediately apparent as is the finer scale of the glycerol flow compared to the two polymer solutions. The impression gained from the two polymer liquid flows is that the streaky structures tend to be longer which is consistent with results in the literature (e.g. [23]).

10. Conclusions

Measurements have been reported for turbulent flow of eight shear-thinning, drag-reducing polymer solutions through a rectangular duct. A novel experimental approach involving a slit cut into the duct surface allowed easy access for LDA measurements of u, u', v' and $-\rho\overline{uv}$. The measurements demonstrate that the slit has negligible effect on the near-wall flow (to $y^+ \approx 1$). The measurements also include w' and so permit the determination of turbulent kinetic energy k in addition to the Reynolds shear and polymer stresses and also the Lumley–Pope anisotropy parameters η and ξ.

The peak values of w'^+ are practically independent of the level of drag reduction whereas those of v'^+ decrease almost linearly by about 40% between zero and 80% drag reduction. The streamwise component of turbulent kinetic energy (in wall units) increases monotonically up to about 50% drag reduction but then shows a more complicated trend with some data showing a further increase while other data suggest that drag reduction is also accompanied by suppression of this component.

The anisotropy data fall remarkably close to the axisymmetric-turbulence side of the Lumley–Pope triangle with maximum values for η and ξ in the near-wall region close to the one-dimensional turbulence limit of 1/3. There is a marked decrease in anisotropy with distance from the near-surface peak in all cases but this tendency progressively reduces with increasing concentration/drag-reduction level.

References

[1] B.A. Toms, Some observations on the flow of linear polymer solutions through straight tubes at large Reynolds numbers, in: Proceedings of the 1st International Congress Rheology 2, North Holland, Amsterdam, 1948, pp. 135–141.
[2] R. Sureshkumar, A.N. Beris, R.A. Handler, Direct numerical simulation of the turbulent channel flow of a polymer solution, Phys. Fluids 9 (3) (1997) 743–755.
[3] J.M.J. Den Toonder, M.A. Hulsen, G.D.C. Kuiken, F.T.M. Nieuwstadt, Drag reduction by polymer additives in a turbulent pipe flow: numerical and laboratory experiments, J. Fluid Mech. 337 (1997) 193–231.
[4] C.D. Dimitropoulos, R. Sureshkumar, R.A. Beris, R.A. Handler, Budgets of Reynolds stress, kinetic energy and streamwise enstrophy in viscoelastic turbulent channel flow, Phys. Fluids 13 (4) (2001) 1016–1027.
[5] E. de Angelis, C.M. Casciola, V.S. L'vov, R. Piva, I. Procaccia, Drag reduction by polymers in turbulent channel flows: Energy redistribution between invariant empirical modes, Phys. Rev. E 67 (5) (2003), 056312:1–11.
[6] T. Min, J.Y. Yoo, H. Choi, D.D. Joseph, Drag reduction by polymer additives in a turbulent channel flow, J. Fluid Mech. 486 (2003) 213–238.
[7] P.R. Resende, M.P. Escudier, F. Presti, F.T. Pinho, D.O.A. Cruz, Numerical predictions and measurements of Reynolds normal stresses in turbulent pipe flow of polymers, Int. J. Heat Fluid Flow 27 (2) (2006) 204–219.
[8] C.-F. Li, V.K. Gupta, R. Sureshkumar, B. Khomani, Turbulent channel flow of dilute polymeric solutions: drag reduction scaling and an eddy viscosity model, J. Non-Newt. Fluid Mech. 139 (2006) 177–189.
[9] F.T. Pinho, B.A. Younis, R. Sureshkumar, A low Reynolds number turbulence closure for viscoelastic liquids, J. Non-Newt. Fluid Mech. 154 (2008) 89–108.
[10] S.E. Logan, Laser velocimeter measurement of Reynolds stress and turbulence in dilute polymer solutions, AIAA J. 10 (7) (1972) 962–964.
[11] M.J. Rudd, Velocity measurements made with a laser dopplermeter on the turbulent pipe flow of a dilute polymer solution, J. Fluid Mech. 51 (4) (1972) 673–685.
[12] B. Gampert, C.K. Yong, Turbulent square duct flow with polymer additives, in: Xth International Congress Rheology 1, Sydney, 1988, pp. 330–332.
[13] B. Gampert, C.K. Yong, The influence of polymer additives on the coherent structure of turbulent channel flow. Structure of turbulence and drag reduction, in: A. Gyr (Ed.), IUTAM Symposium, Zurich/Switzerland, Springer-Verlag, Berlin, Heidelberg, 1990.
[14] M.P. Escudier, S. Smith, Fully developed turbulent flow of non-Newtonian liquids through a square duct, Proc. R. Soc. Lond. A 457 (2001) 911–936.
[15] B. Gampert, T. Braemer, T. Eich, T. Dietmann, Rheo-optical investigations and near-wall turbulence structure of polymer solutions in turbulent channel flow, J. Non-Newt. Fluid Mech. 126 (2–3) (2004) 115–121.
[16] M.M. Reischman, W.G. Tiederman, Laser-Doppler anemometer measurements in drag-reducing channel flows, J. Fluid Mech. 70 (2) (1975) 369–392.
[17] T.S. Luchik, W.G. Tiederman, Turbulent structure in low-concentration drag-reducing channel flows, J. Fluid Mech. 190 (1988) 241–263.
[18] W.W. Willmarth, T. Wei, C.O. Lee, Laser anemometer measurements of Reynolds stress in a turbulent channel flow with drag reducing polymer additives, Phys. Fluids 30 (4) (1987) 933–935.
[19] K.J. Harder, W.G. Tiederman, Drag reduction and turbulent structure in two-dimensional channel flows, Phil. Trans. R. Soc. Lond. A 336 (1991) 19–34.
[20] T. Wei, W.W. Willmarth, Modifying turbulent structure with drag reducing polymer additives in turbulent channel flows, J. Fluid Mech. 245 (1992) 619–641.
[21] B. Gampert, A. Rensch, Polymer concentration and near wall turbulence structure of channel flow of polymer solutions, in: FED 237 ASME Fluids Engineering Division Conference 2, 1996, pp. 129–135.
[22] M.D. Warholic, H. Massah, T.J. Hanratty, Influence of drag-reducing polymers on turbulence: effects of Reynolds number, concentration and mixing, Exp. Fluids 27 (1999) 461–472.
[23] M.D. Warholic, D.K. Heist, M. Katcher, T.J. Hanratty, Study with particle-image velocimetry of the influence of drag-reducing polymers on the structure of turbulence, Exp. Fluids 31 (2001) 474–483.
[24] B. Gampert, A. Delgado, Laser-Doppler-anemometer measurements in turbulent flow of viscoelastic fluids, in: A. Dybbs, P.A. Pfund (Eds.), ASME International Symposium Laser Anemometry, 1985, pp. 143–150.
[25] M.P. Escudier, F. Presti, S. Smith, Drag reduction in the turbulent pipe flow of polymers, J. Non-Newt. Fluid Mech. 81 (3) (1999) 197–213.
[26] R.B. Dean, Reynolds number dependence of skin friction and other flow variables in two-dimensional rectangular duct flow, J. Fluids Eng. 100 (1978) 215–223.
[27] D. Poggi, A. Poroprato, L. Ridolfi, An experimental contribution to near-wall measurements by means of a special laser Doppler anemometry technique, Exp. Fluids 32 (3) (2002) 336–375.
[28] K. Walters, A.Q. Bhatti, N. Mori, The influence of polymer conformation on the rheological properties of aqueous polymer solutions, in: K.D. Dee, P.N. Kaloni, Pitman (Eds.), Recent Developments in Structured Continua, 1990.
[29] K. Yasuda, R.C. Armstrong, R.E. Cohen, Shear flow properties of concentrated solutions of linear and star branched polystyrenes, Rheol. Acta 20 (1981) 163–178.
[30] P.S. Virk, Drag reduction fundamentals, AICh J. 21 (1975) 625–656.
[31] W. Kozicki, C. Tiu, Parametric modelling of flow geometries in non-Newtonian flows, in: N.P. Cheremisinoff (Ed.), Encyclopedia of Fluid Mechanics, vol. 7: Rheology and Non-Newtonian Flows, Gulf Publishing Co., Houston, 1986.
[32] K.D. Housiadas, A.N. Beris, Characteristic scales and drag reduction evaluation in turbulent channel flow of nonconstant viscosity viscoelastic fluids, Phys. Fluids 16 (2004) 1581–1586.
[33] J.L. Lumley, Computational modelling of turbulent flows, Adv. Appl. Mech. 18 (1978) 123–176.
[34] S. Pope, Turbulent Flows, Cambridge University Press, New York, 2000.
[35] J. Jovanović, M. Pashtrapanska, B. Frohnapfel, F. Durst, J. Koskinen, K. Koskinen, On the mechanism responsible for turbulent drag reduction by dilute addition of high polymers: theory, experiments, simulations and predictions, J. Fluids Eng. 128 (2006) 118–130.

Please cite this article in press as: M.P. Escudier, et al., Turbulent flow of viscoelastic shear-thinning liquids through a rectangular duct: Quantification of turbulence anisotropy, J. Non-Newtonian Fluid Mech. (2009), doi:10.1016/j.jnnfm.2009.01.002